A computational homogenization approach for the yield design of periodic thin plates. Part I: Construction of the macroscopic strength criterion

Jérémy Bleyer, Patrick De Buhan

▶ To cite this version:

A computational homogenization approach for the yield design of periodic thin plates
Part I : Construction of the macroscopic strength criterion

Jeremy Bleyer[a,*], Patrick de Buhan[a]

[a]*Université Paris-Est, Laboratoire Navier,*
Ecole des Ponts ParisTech-IFSTTAR-CNRS (UMR 8205)
6-8 av Blaise Pascal, Cité Descartes, 77455 Champs-sur-Marne, FRANCE

Abstract

The purpose of this paper is to propose numerical methods to determine the macroscopic bending strength criterion of periodically heterogeneous thin plates in the framework of yield design (or limit analysis) theory. The macroscopic strength criterion of the heterogeneous plate is obtained by solving an auxiliary yield design problem formulated on the unit cell, that is the elementary domain reproducing the plate strength properties by periodicity. In the present work, it is assumed that the plate thickness is small compared to the unit cell characteristic length, so that the unit cell can still be considered as a thin plate itself. Yield design static and kinematic approaches for solving the auxiliary problem are, therefore, formulated with a Love-Kirchhoff plate model. Finite elements consistent with this model are proposed to solve both approaches and it is shown that the corresponding optimization problems belong to the class of second-order cone programming (SOCP), for which very efficient solvers are available. Macroscopic strength criteria are computed for different type of heterogeneous plates (reinforced, perforated plates,...) by comparing the results of the static and the kinematic approaches. Information on the unit cell failure modes can also be obtained by representing the optimal failure mechanisms. In a companion paper, the so-obtained homogenized strength criteria will be used to compute ultimate loads of global plate structures.

Keywords: yield design, limit analysis, homogenization theory, thin plate model, second-order cone programming, finite element method

1. Introduction

Heterogeneous periodic thin plates are frequently encountered in civil engineering applications and the assessment of their bending strength capacities is of great importance

---

for engineers. The computation of the ultimate load of a structure can be performed using two different class of methods. The first one, called the incremental approach, relies on a step-by-step elasto-plastic computation of the whole loading path until failure. This approach is time consuming, especially for complex structures, and poses convergence issues when approaching the collapse of the structure. The second class concerns direct methods using the theory of limit analysis or, in a more general manner, yield design theory [1] to bracket the ultimate load using two theorems : the lower bound static approach and the upper bound kinematic approach. The efficiency of direct methods is that they require only the verification of equilibrium equations and the fulfillment of the yield criterion at each point of the structure without any knowledge of the mechanical behavior (apart from the strength criterion) or the whole loading path.

The resolution of the static and kinematic approaches requires solving convex nonlinear optimization problems. Numerical methods dedicated to yield design have gained recent attention due to the development of mathematical programming techniques. A traditional approach involves the linearization of the yield criteria so that the corresponding optimization problems can be formulated within linear programming [2–5], for which powerful softwares based on interior point algorithms are available. These algorithms have also been developed for a broader class of optimization problems called second order cone programming (SOCP) [6] and implemented in commercial codes such as the MOSEK software package [7]. Remarkably, a large number of traditional yield criteria can be expressed using conic constraints so that limit analysis problems can be formulated within SOCP [8]. Recent works applied this method to 2D plane strain problems [9, 10], frame structures or thin plates in bending [11, 12]. The obtained results seem very promising in terms of computational time saving (problems with a large number of optimization variables can be solved within seconds) as well as accuracy. For these reasons, these numerical methods will be used in this work.

Despite the efficiency of the previously mentioned numerical procedures, yield design of periodic media can be very difficult to perform due to the presence of rapidly and strongly varying material properties on a large scale structure. Numerical computations on the heterogeneous structure are, therefore, out of reach due to the high degree of local refinement needed to correctly capture the properties of the inhomogeneities. Homogenization theory in yield design has therefore been developed to characterize the strength domain of an equivalent homogeneous media with the idea that the corresponding homogenized yield design problem would, then, be much easier to solve. Founding works are due to Suquet [13] and de Buhan [14].

The determination of the homogenized or macroscopic strength properties are quite similar to homogenization theory in elasticity. The macroscopic strength domain is, indeed, determined by solving an auxiliary yield design problem formulated on the unit cell of the periodic plate. Homogenization of elastic in-plane periodic plates has been widely studied by different authors. One main feature of this problem is that a plate model is valid in the limit of a small thickness h compared to the typical length L of the plate structure whereas the homogenization procedure is valid in the limit of a small in-plane typical length a of the unit cell compared to the same length L. Therefore, different homogenization procedures

have to be considered depending on the relative values of a and h.

For instance, if a and h are of the same order, the unit cell has to be modeled as a 3D medium [15–17]. On the contrary, if h is small compared to a, it is possible to replace the original 3D heterogeneous body by a 2D heterogeneous Love-Kirchhoff plate, which is homogenized in a second step (see [18] for elastic plates). Our work will be focused on this specific case within the framework of yield design theory and associated numerical methods.

This paper is organized as follows : in section 2, the homogenization theory in yield design will be briefly described within the framework of thin plates in bending and the equilibrium equations of the associated Love-Kirchhoff plate model will be recalled. Section 3 is devoted to the formulation of the auxiliary yield design problem, either by the static approach or by the kinematic approach, and the definition of the macroscopic strength criterion G^{hom} is given. Numerical methods to solve the static approach are then presented in section 4 and the corresponding optimization problem is formulated as a SOCP problem. Section 5 deals with the case of the kinematic approach in the same manner. Finally, different numerical examples are studied in section 6, in order to assess the performance of both numerical procedures.

2. Yield design of periodic thin plates : a homogenization approach

2.1. The heterogeneous problem

We consider a heterogeneous thin plate occupying a domain Ω in the $(x, y)-$plane. Internal forces of the plate are the tensor of membrane forces $\underline{\underline{N}}$, the tensor of bending moments $\underline{\underline{M}}$ and the vector of shear forces $\underline{V}$. Generally speaking, the set of admissible internal forces with respect to the local strength of the plate at a point $\underline{x} \in \Omega$ can be represented as a bounded convex set $G(\underline{x})$:

$$(\underline{\underline{N}}, \underline{\underline{M}}, \underline{V}) \in G(\underline{x})$$

In the special case of thin plates in bending, it is generally assumed that the plate is *infinitely resistant to both membrane and shear forces* such that the local strength criterion depends on the bending moment only :

$$\underline{\underline{M}} \in G(\underline{x})$$

Now, assuming that the plate loading depends upon several loading parameters $\underline{Q}$, the domain Λ of potentially safe loads $\underline{Q}$ is defined as the set of loads such that there exists a statically admissible (S.A.) bending moment field $\underline{\underline{M}}(\underline{x})$ (i.e. which equilibrates the loading $\underline{Q}$), satisfying the strength criterion at each point of the plate (see [1]) :

$$\Lambda = \left\{ \underline{Q} \mid \exists \underline{\underline{M}}(\underline{x}) \text{ S.A. with } \underline{Q}, \ \forall \underline{x} \in \Omega \quad \underline{\underline{M}}(\underline{x}) \in G(\underline{x}) \right\}$$

Making use of the virtual work principle, one can obtain a kinematic definition of Λ, dual to the previous static one. In the case of thin plates in bending, the hypothesis of infinite membrane and shear strength imposes that the plate kinematics obey the Love-Kirchhoff condition. Let $\widehat{u}$ be the virtual transversal velocity of the plate and $\underline{q}$ the generalized

kinematic parameters defined by duality in the expression of the work of external forces, such that for all $\widehat{u}$ kinematically admissible (K.A.) with $\underline{q}$ (i.e. piecewise continuous and differentiable satisfying the kinematic boundary conditions), the virtual work of external load is given by $P_{ext}(\widehat{u}) = \underline{Q} \cdot \underline{q}$. We then introduce $\pi(\widehat{\underline{\underline{\chi}}}; \underline{x})$, the support function of $G(\underline{x})$ defined as

$$\pi(\widehat{\underline{\underline{\chi}}}; \underline{x}) = \sup_{\underline{\underline{M}} \in G(\underline{x})} \underline{\underline{M}} : \widehat{\underline{\underline{\chi}}}$$

and the associated maximum resisting work $P_{rm}(\widehat{u})$ as follows[1] :

$$P_{rm}(\widehat{u}) = \int_{\Omega} \pi(\widehat{\underline{\underline{\chi}}}; \underline{x}) d\Omega$$

where $\widehat{\underline{\underline{\chi}}} = \underline{\underline{\nabla}}_s \nabla \widehat{u}(\underline{x})$ is the curvature tensor associated with the virtual velocity field $\widehat{u}$. The following kinematic definition of Λ is then obtained :

$$\underline{Q} \in \Lambda \Longrightarrow \forall \widehat{u} \text{ K.A. with } \underline{q}, \quad P_{ext}(\widehat{u}) \leq P_{rm}(\widehat{u})$$

2.2. The homogenized problem

Now, the special case of plates which are periodic in their in-plane direction will be considered. Therefore, there exist two vectors $\underline{a}_1, \underline{a}_2$ such that $G(\underline{x})$ can be reproduced by periodicity along $\underline{a}_1$ and $\underline{a}_2$:

$$G(\underline{x} + n_1 \underline{a}_1 + n_2 \underline{a}_2) = G(\underline{x}) \quad \forall \underline{x} \in \Omega, \forall n_1, n_2 \in \mathbb{Z}$$

The two vectors $\underline{a}_1$ and $\underline{a}_2$ define the unit cell of the periodic plate. In the case when the typical size a of the unit cell is small in comparison to the plate typical length L ($a \ll L$), the natural idea of homogenization theory is to substitute the local heterogeneous strength criterion $G(\underline{x})$ by a homogenized or macroscopic strength criterion G^{hom}, as illustrated in figure 1.

Using the same definitions as before, we introduce

$$\Lambda^{hom} = \left\{ \underline{Q} \mid \exists \underline{\underline{M}}(\underline{x}) \text{ S.A. with } \underline{Q}, \forall \underline{x} \in \Omega \quad \underline{\underline{M}}(\underline{x}) \in G^{hom} \right\}$$

which also admits the following kinematic definition :

$$\underline{Q} \in \Lambda^{hom} \Longrightarrow \forall \widehat{u} \text{ K.A. with } \underline{q} \quad P_{ext}(\widehat{u}) \leq P_{rm}^{hom}(\widehat{u}) = \int_{\Omega} \Pi_{hom}(\widehat{\underline{\underline{\chi}}}) d\Omega$$

---

[1]This expression assumes that the rotation vector associated with the gradient of the transversal velocity field $\widehat{u}$ is everywhere continuous. If this is not the case, another term taking into account the contribution of angular jumps has to be considered in the expression of the maximum resisting work. For more details, we refer to [12] and section 5.
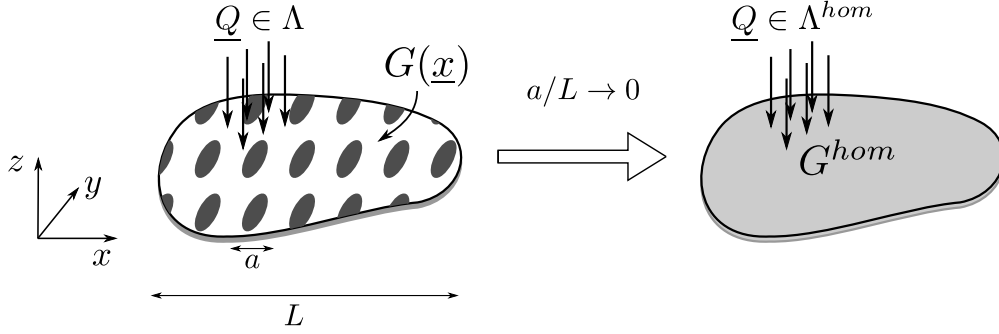
Figure 1: Illustration of the homogenization procedure for a periodic heterogeneous thin plate : initial heterogeneous (left) and equivalent homogeneous (right) yield design plate problems

where $\Pi_{hom}(\widehat{\underline{\underline{\chi}}})$ is the support function associated with G^{hom}.

Similarly to the case of 3D periodic heterogeneous media [13, 14], the following result of homogenization theory in yield design holds true :

$$\Lambda \longrightarrow \Lambda^{hom} \quad \text{when } a/L \to 0$$

Let mention that Γ-convergence results for the homogenization of rigid perfectly plastic periodic thin plates in the case $a \ll L$ are given in [19].

2.3. Love-Kirchhoff plate model

Since the plate is supposed to be infinitely resistant to shear forces, the virtual motions of the plate must satisfy the Love-Kirchhoff condition.

In this case, the weak form of the Love-Kirchhoff plate equations is obtained by writing the virtual work of internal forces for a continuously differentiable test function $u(\underline{x})$ (transversal velocity) and integrating twice by parts :

$$P_{int}(u) = -\int_\Omega \underline{\underline{M}} : \underline{\nabla}_s \underline{\nabla} u d\Omega = \int_\Omega \text{div } \underline{\underline{M}} \cdot \underline{\nabla} u d\Omega - \int_{\partial\Omega} (\underline{\underline{M}} \cdot \underline{n}) \cdot \underline{\nabla} u dl + \int_\Gamma [\![\underline{\underline{M}} \cdot \underline{n}]\!] \cdot \underline{\nabla} u dl$$

$$\begin{aligned} P_{int}(u) = \quad & -\int_\Omega \text{div}\,(\text{div } \underline{\underline{M}}) u d\Omega + \int_{\partial\Omega} (\text{div } \underline{\underline{M}} \cdot \underline{n}) u dl - \int_\Gamma [\![\text{div } \underline{\underline{M}} \cdot \underline{n}]\!] u dl \\ & -\int_{\partial\Omega} (\underline{\underline{M}} \cdot \underline{n}) \cdot \underline{\nabla} u dl + \int_\Gamma [\![\underline{\underline{M}} \cdot \underline{n}]\!] \cdot \underline{\nabla} u dl \end{aligned}$$

where Γ is a line of potential discontinuities in Ω, $\underline{n}$ a unit normal vector and where $[\![\cdot]\!]$ represents the discontinuity of the quantity $(\cdot)$ through Γ following its normal $\underline{n}$. In the case when the loading consists only of a distributed transversal pressure $p(\underline{x})$, the virtual work of external forces is given by $P_{ext}(u) = -\int_\Omega p(\underline{x})u(\underline{x})d\Omega$. Then, the virtual work principle reads :

$$0 = P_{int}(u) + P_{ext}(u) \quad \forall u \text{ K.A.}$$

5

The weak formulation yields the following equilibrium equation :

$$\text{div}\,(\text{div}\,\underline{\underline{M}}) + p = 0 \quad \text{in}\ \Omega$$

While the boundary conditions and jump equations require a specific attention because of the fact that, on a given line, u and $\underline{\nabla u}\cdot\underline{n}$ are independent fields whereas u and $\underline{\nabla u}\cdot\underline{t}$ are not ($\underline{t}$ being a unit tangent vector). For example, on the part of the boundary where $u = \underline{\nabla u}\cdot\underline{n} = 0$, it is impossible to choose an arbitrary value of $\underline{\nabla u}\cdot\underline{t}$ to obtain the boundary condition $M_{nt} = 0$. This specific aspect has been widely reported in the literature and one method to overcome this problematic aspect is to use the following equality $M_{nt}\partial_t u = \partial_t(M_{nt}u) - (\partial_t M_{nt})u$ in the variational form, here ∂_t denotes the derivative along the tangential direction. Introducing

$$K = (\text{div}\,\underline{\underline{M}})\cdot\underline{n} + \frac{\partial M_{nt}}{\partial t}$$

as the *equivalent Kirchhoff shear force*, one obtains :

$$P_{int}(u) = \ -\int_\Omega \text{div}\,(\text{div}\,\underline{\underline{M}})u d\Omega + \int_{\partial\Omega} Ku dl - \int_\Gamma [\![K]\!]u dl - \int_{\partial\Omega} M_{nn}\partial_n u dl$$
$$+ \int_\Gamma [\![M_{nn}]\!]\partial_n u dl - \int_{\partial\Omega} \partial_t(M_{nt}u)dl + \int_\Gamma [\![\partial_t(M_{nt}u)]\!]dl$$

If $\partial\Omega \cup \Gamma$ is regular except on a finite number of angular points c_j, the last two terms can be rewritten as :

$$-\int_{\partial\Omega} \partial_t(M_{nt}u)dl + \int_\Gamma [\![\partial_t(M_{nt}u)]\!]dl = -\sum_j R_j u(c_j)$$

where $R_j = [\![M_{nt}(c_j)]\!]$ is the discontinuity of M_{nt} at a corner c_j.
Finally, the variational formulation reduces to : $\forall u K.A.$

$$0 = \int_\Omega (\text{div}\,(\text{div}\,\underline{\underline{M}}) + p)u d\Omega + \int_{\partial\Omega}(M_{nn}\partial_n u - Ku)dl - \int_\Gamma([\![M_{nn}]\!]\partial_n u - [\![K]\!]u)dl + \sum_j R_j u(c_j)$$

The variational formulation is now written in terms of independent fields only and one can obtain the following boundary conditions :

$$
\begin{array}{lll}
K = 0 & M_{nn} = 0 & \text{on}\ \partial\Omega_1 \\
K = 0 & \partial_n u = 0 & \text{on}\ \partial\Omega_2 \\
u = 0 & M_{nn} = 0 & \text{on}\ \partial\Omega_3 \\
u = 0 & \partial_n u = 0 & \text{on}\ \partial\Omega_4
\end{array}
\qquad \partial\Omega = \bigcup_i \partial\Omega_i, \partial\Omega_i \cap \partial\Omega_j = \emptyset\ \text{for}\ i \neq j
$$

and the following jump equations (figure 2):

$$
\begin{array}{ll}
[\![M_{nn}]\!] = 0 & \\
[\![K]\!] = 0 & \text{through}\ \Gamma \\
R_j = [\![M_{nt}(c_j)]\!] = 0 & \text{at}\ c_j
\end{array}
$$

$$\llbracket M_{nn} \rrbracket = M_{nn}^+ - M_{nn}^- = 0$$
$$\llbracket K \rrbracket = K^+ - K^- = 0$$

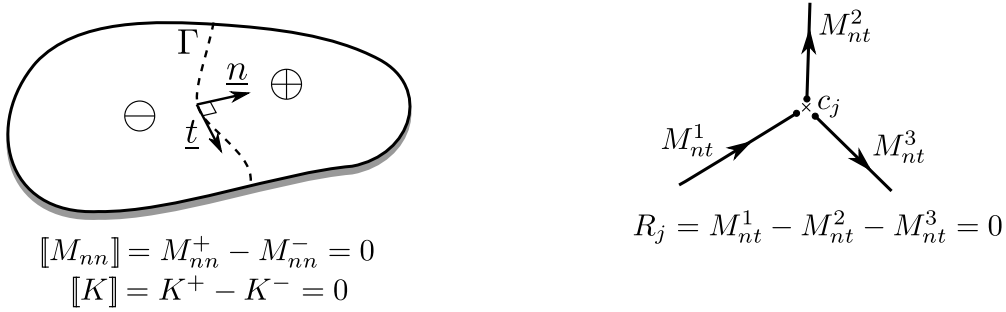$$R_j = M_{nt}^1 - M_{nt}^2 - M_{nt}^3 = 0$$

Figure 2: Jump equations of the Love-Kirchhoff plate model : through a line Γ (left) and at a corner c_j (right)

3. Determination of G^{hom} by solving an auxiliary yield design problem

The process of determining the macroscopic strength criterion G^{hom} requires to solve a specific auxiliary yield design problem formulated on the unit cell, allowing to relate macroscopic quantities to the microscopic ones. Obviously, it is to be recalled that the thin plate model is only an idealization of a 3D structure in the limit of a small thickness h compared to the characteristic length of the structure L. As already mentioned in the introduction, the present paper is interested in the case when the thickness h can still be considered as small when compared to the typical size of the unit cell : $h \ll a \ll L$. In this specific case, the original 3D unit cell problem can still be modeled as a plate problem.

3.1. Space of statically admissible moment fields and definition of G^{hom}

Let $\mathcal{A}$ be such a unit cell of the periodic plate, $\underline{\xi}$ a point in $\mathcal{A}$ and Γ a potential discontinuity line in $\mathcal{A}$. $\underline{\underline{M}}$ is the macroscopic bending tensor which will play the role of loading parameters for the auxiliary problem.

The appropriate conditions to formulate a correct auxiliary problem in the framework of periodic homogenization theory are the following :

- zero distributed forces;

- periodic conditions on the boundary of the unit cell (see figure 3);

- averaging relation relating the macroscopic to the microscopic bending moment tensors.

Hence, we introduce the set $SA(\underline{\underline{M}})$ of local bending moment tensor $\underline{\underline{m}}(\underline{\xi})$ defined on the unit cell which are statically admissible with $\underline{\underline{M}}$ as follows :
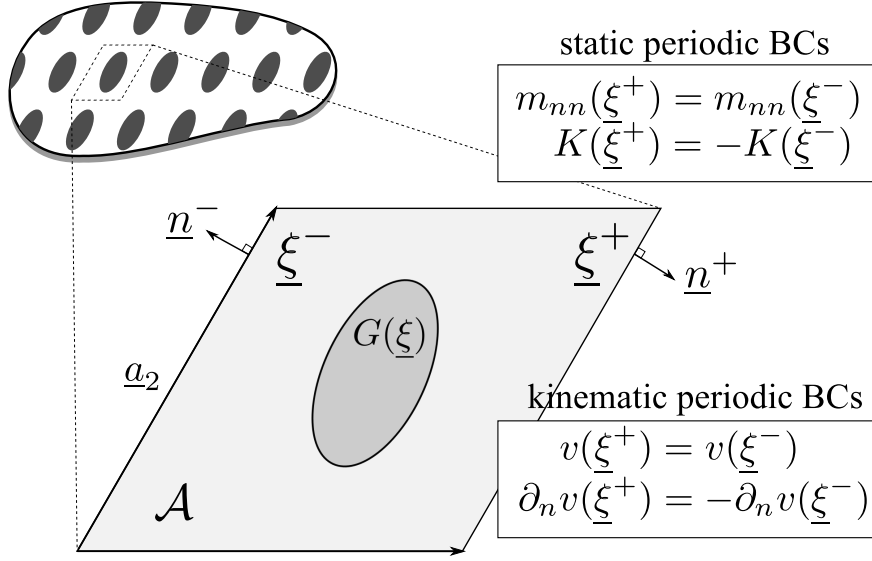
Figure 3: Periodic and antiperiodic boundary conditions on the unit cell for static and kinematic fields. $\underline{\xi}^+$ and $\underline{\xi}^-$ are the position vectors of two points on opposite sides of the unit cell and deduced from each other by periodicity.

$$\underline{m}(\underline{\xi}) \in SA(\underline{\underline{M}}) \Longleftrightarrow \begin{vmatrix} \text{div div } \underline{\underline{m}}(\underline{\xi}) = 0 & \text{in } \mathcal{A} & (1) \\ [\![m_{nn}]\!] = 0 & \text{through } \Gamma & (2) \\ [\![K]\!] = 0 & \text{through } \Gamma & (3) \\ R_j = 0 & \text{at } c_j \text{ inside } \mathcal{A} & (4) \\ m_{nn} & \mathcal{A} - \text{periodic} & (5) \\ K & \mathcal{A} - \text{antiperiodic} & (6) \\ R_j & \mathcal{A} - \text{antiperiodic} & (7) \\ \underline{\underline{M}} = \langle \underline{\underline{m}}(\underline{\xi}) \rangle & & (8) \end{vmatrix}$$

where $\langle \cdot \rangle = \dfrac{1}{|\mathcal{A}|} \displaystyle\int_{\mathcal{A}} (\cdot) dA$.

The macroscopic strength criterion G^{hom} is then obtained as follows :

$$G^{hom} = \left\{ \underline{\underline{M}} \mid \exists \underline{\underline{m}}(\underline{\xi}) \in SA(\underline{\underline{M}}), \ \forall \underline{\xi} \in \mathcal{A} \quad \underline{\underline{m}}(\underline{\xi}) \in G(\underline{\xi}) \right\} \tag{9}$$

which states that the macroscopic strength domain consists of all the macroscopic bending moments for which there exists at least one microscopic bending moment distribution on the unit cell which is statically admissible with the macroscopic bending moment, while fulfilling the local strength criterion at each point of the unit cell.

3.2. Space of kinematically admissible velocity fields

Let $KA(\underline{\underline{\chi}})$ bet the set of local transversal velocity fields $u(\underline{\xi})$ defined on the unit cell, and kinematically admissible with a macroscopic curvature tensor $\underline{\underline{\chi}}$ as follows :

$$u(\underline{\xi}) \in KA(\underline{\underline{\chi}}) \iff \left| \begin{array}{llr} u(\underline{\xi}) = \dfrac{1}{2}\underline{\xi} \cdot \underline{\underline{\chi}} \cdot \underline{\xi} + v(\underline{\xi}) & \text{in } \mathcal{A} & (10) \\[2mm] v(\underline{\xi}) & \text{continuous in } \mathcal{A} & (11) \\[2mm] v(\underline{\xi}) & \mathcal{A} - \text{periodic} & (12) \\[2mm] \dfrac{\partial v}{\partial n}(\underline{\xi}) & \mathcal{A} - \text{antiperiodic} & (13) \end{array} \right.$$

This definition deserves some remarks :

- Due to the previous assumptions (Love-Kirchhoff kinematics), the following properties can be deduced :

  - $u(\underline{\xi})$ is continuous;
  - the discontinuity of the gradient $\underline{\nabla u}$ through a discontinuity line Γ is necessarily normal to this line by virtue of Hadamard's compatibility condition [20]. Hence : $[\![\underline{\nabla u}]\!] = \left[\!\!\left[\dfrac{\partial v}{\partial n}\right]\!\!\right] \underline{n}$
  - $\underline{\nabla v}(\underline{\xi})$ is $\mathcal{A}-$periodic.

- Assumptions made on $v(\underline{\xi})$ are consistent with Love-Kirchhoff kinematics. In particular, the local velocity field u can be seen as a Love-Kirchhoff velocity field obtained by the superposition of a homogeneous curvature term plus a periodic perturbation $v(\underline{\xi})$.

- Rotation of the microstructure is characterized by the gradient of u : $\underline{\nabla u}(\underline{\xi}) = \underline{\underline{\chi}} \cdot \underline{\xi} + \underline{\nabla v}(\underline{\xi})$ which is also obtained by the superposition of a homogeneous curvature term plus a periodic perturbation $\underline{\nabla v}(\underline{\xi})$ of the rotation vector.

- The local curvature is $\underline{\underline{\kappa}}(\underline{\xi}) = \underline{\underline{\nabla_s \nabla u}} = \underline{\underline{\chi}} + \underline{\underline{\nabla_s \nabla v}}(\underline{\xi})$. Using Green's theorem, its average is given by :

$$\begin{aligned} \langle \underline{\underline{\kappa}} \rangle &= \underline{\underline{\chi}} + \langle \underline{\underline{\nabla_s \nabla v}} \rangle \\ &= \underline{\underline{\chi}} + \frac{1}{|\mathcal{A}|}\left(\int_{\partial A} \frac{1}{2}(\underline{\nabla v} \otimes \underline{n} + \underline{n} \otimes \underline{\nabla v})dl - \int_{\Gamma} \frac{1}{2}([\![\underline{\nabla v}]\!] \otimes \underline{n} + \underline{n} \otimes [\![\underline{\nabla v}]\!])dl \right) \end{aligned}$$

the first term vanishes because $\underline{\nabla v} \otimes \underline{n}$ is anti-periodic. Thus, the following identity holds true :

$$\underline{\underline{\chi}} = \langle \underline{\underline{\kappa}} \rangle + \frac{1}{|\mathcal{A}|} \int_{\Gamma} \left[\!\!\left[\frac{\partial v}{\partial n}\right]\!\!\right] \underline{n} \otimes \underline{n}\, dl \qquad (14)$$

Using the virtual work principle, it is quite easy to see that the two sets $SA(\underline{M})$ and $KA(\underline{\underline{\chi}})$ are in duality in the following sense :

$$\forall \underline{m} \in SA(\underline{M}), \forall u \in KA(\underline{\underline{\chi}}) \quad P_{ext}(u) = |\mathcal{A}| \left\langle \underline{m} : \underline{\underline{\kappa}}(\underline{\xi}) \right\rangle = |\mathcal{A}|\underline{M} : \underline{\underline{\chi}}$$

i.e. the average internal work on the unit cell is equal to the internal work of the average bending moment $\underline{M}$ and of the macroscopic curvature tensor $\underline{\underline{\chi}}$. More precisely, owing to

9

(14) in the case when there are no rotation discontinuities of the velocity field on the unit cell, $\underline{\underline{\chi}}$ is equal to the average of the local curvature $\langle \underline{\underline{\kappa}}(\xi) \rangle$ such that the previous relation can now be written :

$$\left\langle \underline{\underline{m}} : \underline{\underline{\kappa}}(\xi) \right\rangle = \left\langle \underline{\underline{m}}(\xi) \right\rangle : \left\langle \underline{\underline{\kappa}}(\xi) \right\rangle = \underline{\underline{M}} : \underline{\underline{\chi}}$$

This expression can be interpreted as a generalized Hill's lemma which is the basis of all homogenization procedures. In our case, $\underline{\underline{M}}$ clearly appears as a three-parameter (M_{xx}, M_{yy}, M_{xy}) loading mode, the associated dual kinematic parameters being the three components of the macroscopic curvature tensor $(\chi_{xx}, \chi_{yy}, \chi_{xy})$.

3.3. Kinematic definition of G^{hom}

Using the previous notations, it can be shown that the macroscopic support function Π_{hom} is given by :

$$\Pi_{hom}(\underline{\underline{\chi}}) = \sup_{\underline{\underline{M}} \in G^{hom}} \underline{\underline{M}} : \underline{\underline{\chi}} = \inf_{u \in KA(\underline{\underline{\chi}})} \frac{1}{|\mathcal{A}|} \left(\int_{\mathcal{A}} \pi(\underline{\underline{\kappa}}; \xi) dA + \int_{\Gamma} \pi([\![\nabla u]\!]; \underline{n}) dl \right)$$

or introducing KA_0 such that $KA(\underline{\underline{\chi}}) = \left\{ \frac{1}{2} \xi \cdot \underline{\underline{\chi}} \cdot \xi \right\} \oplus KA_0$:

$$\Pi_{hom}(\underline{\underline{\chi}}) = \inf_{v \in KA_0} \frac{1}{|\mathcal{A}|} \left(\int_{\mathcal{A}} \pi(\underline{\underline{\chi}} + \underline{\underline{\nabla}}_s \nabla v; \xi) dA + \int_{\Gamma} \pi \left(\left[\!\left[\frac{\partial v}{\partial n} \right]\!\right]; \underline{n} \right) dl \right) \tag{15}$$

Using this kinematic definition, G^{hom} can then be computed as the convex hull of all hyperplanes of equation $\underline{\underline{M}} : \underline{\underline{\chi}} = \Pi_{hom}(\underline{\underline{\chi}})$ for all macroscopic curvatures $\underline{\underline{\chi}}$. Note that, since G has been supposed to be bounded, G^{hom} is also bounded (see definition (9)). Therefore, all suprema and infima in the previous relations are finite and there is no additional condition on the virtual curvatures to ensure finite upper bounds in the kinematic approach.

3.4. Conclusion

In this section, an appropriate definition for the macroscopic strength criterion G^{hom} of a periodic plate has been given. This definition relies upon the solution of an auxiliary yield design problem defined over the unit cell, with specific periodic boundary conditions. This problem can be solved either in its static or its kinematic form. In practice, none of the two problems can be solved analytically and numerical procedures are required based for instance upon the discretization of both problems.

Let $SA_d(\underline{\underline{M}}) \subseteq SA(\underline{\underline{M}})$ and $KA_{0d} \subseteq KA_0$ be subspaces consistent with the previous definitions. If (9) is solved using $SA_d(\underline{\underline{M}})$, one would obtain a lower bound approximation G^{hom}_{stat} to the macroscopic strength criterion G^{hom}. Similarly, if (15) is solved using KA_{0d}, one would obtain a larger value of the macroscopic support function $\Pi^{kin}_{hom} \geq \Pi_{hom}$, corresponding to an upper bound approximation $G^{hom}_{kin} \supset G^{hom}$ to the macroscopic strength criterion. Obvisouly, using the lower (resp. upper) approximation of G^{hom} in the global computation of a homogenized structure will lead to a lower bound (resp. upper bound) of the exact
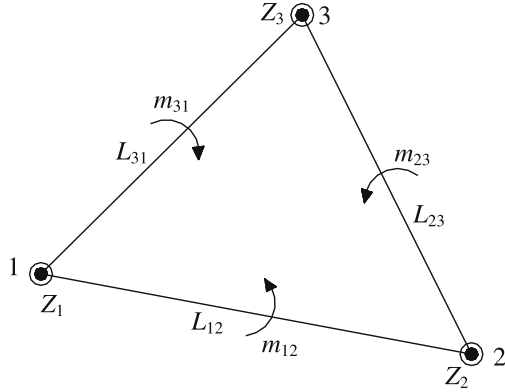
Figure 4: Equilibrium Morley finite element (from [11])

homogenized limit load.

Such numerical procedures based on the finite element method are discussed in the next two sections and it will be shown, on numerical examples, that the obtained approximations of G^{hom} are very close estimates of the exact macroscopic strength criterion.

4. Numerical resolution of the static approach

In this section, the static problem (9) is discretized using the finite element method and the resulting optimization problem is solved using second-order cone programming. Lower bound limit analysis of thin plate problems have already been successfully solved using such methods [11]. Since the present auxiliary problem is very similar to yield design problems formulated on plate structures, the formulations will be simply adapted to take periodic boundary conditions and averaging relations into account.

4.1. Finite element discretization

In the following, the unit cell $\mathcal{A}$ is discretized into N_E triangular finite elements assuming a constant varying moment field in each element [11, 21]. Each such element, known as the equilibrium Morley element, exhibits three degrees of freedom $\{m_e\} = \{m_{xx}\, m_{yy}\, m_{xy}\}^T$ per element. Despite its apparent simplicity, some difficulties may arise for yield design problems involving for instance uniformly distributed pressures, since the Morley element does not result in an exact equilibrium relation for such loadings. In that case, some modifications are required, as mentioned in [11]. However, since in the specific case of periodic homogenization all distributed loads are supposed to be zero, such modifications are unnecessary.

With constant moments, equations (1), (3) and (6) are identically satisfied. Hence, the generalized forces consist of three internal corner forces Z_1, Z_2, Z_3 and three constant normal bending moments along edges m_{12}, m_{23}, m_{31} (figure 4). These generalized forces (collected in a vector $\{G\}$) are related to the moment field in the element $\{m_e\}$ by a constant matrix

11

$[C_e]$ depending on the geometry of the element :

$$\{G\} = [C_e]\{m_e\}$$

If $\{m\}$ collects the degrees of freedom of all N_E elements, the global equilibrium of the unit cell is obtained by assembling all contributions into the following relation :

$$[C]\{m\} = \{0\}$$

thereby satisfying (2) and (4) exactly. It should be mentioned that, in the global equilibrium matrix $[C]$, the equilibrium of edges and nodes belonging to the unit cell boundary are not taken into account. The latter require, indeed, a special treatment to impose the periodic boundary conditions (5) and (7).

Let an edge belonging to the boundary of the unit cell be indexed by i, and let e be the index of its corresponding element. Let i' (resp. e') be the index of the edge (resp. of its corresponding element) on the opposite boundary[2]. The two normal moments on i and i' can then be obtained as :

$$m_{nn}^{(i)} = \langle c_e \rangle \{m_e\} \quad m_{nn}^{(i')} = \langle c_{e'} \rangle \{m_{e'}\}$$

The periodicity of m_{nn} is then enforced by the following condition :

$$m_{nn}^{(i)} - m_{nn}^{(i')} = \langle c_e \rangle \{m_e\} - \langle c_{e'} \rangle \{m_{e'}\} = 0$$

The same kind of equation can be written concerning corner loads for all pair of opposite nodes. Both equations are then assembled into a global matrix $[P]$ taking into account all periodic boundary conditions :

$$[P]\{m\} = \{0\}$$

Finally, if a_e is the area of element number e and $[I_3]$ the 3×3 identity matrix, the averaging condition (8) may be written as :

$$\{M\} = \begin{Bmatrix} M_{xx} \\ M_{yy} \\ M_{xy} \end{Bmatrix} = \frac{1}{|\mathcal{A}|} \begin{bmatrix} a_1[I_3] & a_2[I_3] & \dots & a_{N_E}[I_3] \end{bmatrix} \{m\} = [A]\{m\}$$

From now on, the unit cell will be considered of area $|\mathcal{A}| = 1$.

Finally, it should be mentioned that all equations defining $SA(\underline{M})$ have been exactly satisfied by the proposed discretization. Therefore, if $SA_d(\underline{M})$ is the set of vectors $\{m\}$ satisfying all the previous discretized equations, the following inclusion $SA_d(\underline{M}) \subset SA(\underline{M})$ holds true.

---

[2]Obviously, two opposite boundaries must have exactly the same mesh so that periodic boundary conditions can be imposed.

4.2. Formulation as a standard second-order cone programming problem

The bending moment field has to satisfy the local strength criterion $G(\underline{\xi})$ at each point $\underline{\xi} \in \mathcal{A}$. In the following, it will be assumed that the unit cell is made of materials obeying the von Mises criterion :

$$G(\underline{\xi}) = \left\{ \underline{\underline{m}}(\underline{\xi}) \mid \sqrt{m_{xx}^2 + m_{yy}^2 - m_{xx}m_{yy} + 3m_{xy}^2} - m_p(\underline{\xi}) \le 0 \right\} \tag{16}$$

where $m_p(\underline{\xi})$ is the ultimate bending moment[3] characterizing the strength of the plate at point $\underline{\xi}$.

Since $\underline{\underline{m}}(\underline{\xi})$ is constant over each element e, the yield criterion will be satisfied if :

$$\sqrt{\{m_e\}^T [P_{vM}]\{m_e\}} - m_{p,e} \le 0 \quad \text{with } [P_{vM}] = \begin{bmatrix} 1 & -1/2 & 0 \\ -1/2 & 1 & 0 \\ 0 & 0 & 3 \end{bmatrix}$$

where $m_{p,e} = \inf m_p(\underline{\xi})$ for $\underline{\xi}$ in the element e. In the numerical examples, $m_p(\underline{\xi})$ will be taken equal to a constant $m_{p,e}$ in each element.

Since $[P_{vM}]$ is positive definite, the yield criterion can be formulated as the following conic constraint :

$$\|[J_1]\{m_e\}\| \le m_{p,e}$$

where $[J_1] = \begin{bmatrix} 1 & -1/2 & 0 \\ 0 & \sqrt{3}/2 & 0 \\ 0 & 0 & \sqrt{3} \end{bmatrix}$ is the Cholesky factor of $[P_{vM}]$.

Let us mention that, although only the von Mises criterion will be used in the following, our study can be easily extended to other types of bending plate criteria, provided they can be formulated using conic constraints [8, 12]. This is the case for the Johansen square criterion, the Tresca criterion, etc...

Since $G^{hom} \subset \mathbb{R}^3$, it will be numerically obtained by considering a specific unitary direction $\{M_0\} \in \mathbb{R}^3$, $\|\{M_0\}\| = 1$ and a loading parameter λ such that $\{M\} = \lambda\{M_0\}$. Thus, the static approach reduces to the resolution of the following maximization problem :

$$\begin{aligned}
\lambda_s = \quad & \max \lambda \\
& \text{s.t.} \begin{bmatrix} 0 & [C] \\ 0 & [P] \\ \{M_0\} & -[A] \end{bmatrix} \left\{ \begin{matrix} \lambda \\ \{m\} \end{matrix} \right\} = \left\{ \begin{matrix} 0 \\ 0 \\ 0 \end{matrix} \right\} \\
& \|[J_1]\{m_e\}\| \le m_{p,e} \quad \forall e = 1, \dots, N_E
\end{aligned} \tag{17}$$

This maximization problem is a second-order cone programming (SOCP) problem involving linear equality constraints and N_E conic constraints.

---

[3]$m_p(\underline{\xi}) = \sigma_0(\underline{\xi})h^2/4$ if σ_0 is the uniaxial yield strength of the plate material
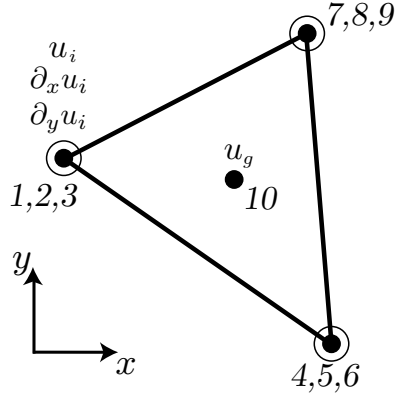
Figure 5: H3 finite element (from [12])

Finally, since $SA_d(\underline{\underline{M}}) \subset SA(\underline{\underline{M}})$ and since the strength criterion is exactly satisfied over the whole unit cell, it can be concluded that $\lambda_s\{M_0\} \in G^{hom}$. Therefore, the convex hull of all $\lambda_s\{M_0\}$ for different values of the direction $\{M_0\}$ defines a lower bound approximation $G^{hom}_{stat} \subset G^{hom}$.

5. Numerical resolution of the kinematic approach

The development of efficient finite elements for the upper bound kinematic approach of thin plates in bending was the main contribution of [12]. More precisely, the present authors proposed to use non-conforming finite elements which incorporate not only curvature-type deformations, but also rotation discontinuities across element edges. In particular, the cubic Hermite triangle (H3) seems to be a very efficient element in terms of numerical accuracy as well as computational time saving. This element will, therefore, be used to solve (15). Some slight modifications will be made to incorporate the specific features of (15); for more details on the other aspects of the formulation, we refer to [12].

5.1. Finite element discretization

The cubic Hermite triangle (H3) is a non-conforming finite element assuming a cubic variation of the transversal displacement, ensuring C^0-continuity. It has 10 degrees of freedom : the transversal displacement and its two derivative along x and y at corner nodes plus the transverse displacement at the centroid (figure 5).

In fact, in our case, the unknown will not be the total velocity $u(\underline{\xi})$ but the periodic fluctuation $v(\underline{\xi})$, as the implementation seemed simpler this way. Let $\{V\}$ be the vector collecting all degrees of freedom. The curvature associated with $v(\underline{\xi})$ at a point $\underline{\xi}$ in e is

computed using a matrix $[B(\underline{\xi})]$ involving second derivatives of shape functions :

$$
\begin{Bmatrix} \partial_{xx}v \\ \partial_{yy}v \\ 2\partial_{xy}v \end{Bmatrix} = [B(\underline{\xi})]\{V\}
$$

The total curvature is then obtained by adding the constant term $\{\chi\}$ due to the macroscopic curvature :

$$
\{\kappa\} = \begin{Bmatrix} \kappa_{xx} \\ \kappa_{yy} \\ 2\kappa_{xy} \end{Bmatrix} = \{\chi\} + [B(\underline{\xi})]\{V\}
$$

In the case of a von Mises criterion, the local support function writes :

$$
\pi(\underline{\underline{\kappa}}; \underline{\xi}) = \frac{2m_p}{\sqrt{3}}(\underline{\xi})\sqrt{\kappa_{xx}^2 + \kappa_{yy}^2 + \kappa_{xx}\kappa_{yy} + \kappa_{xy}^2}
$$

As before, this expression can be written as :

$$
\pi(\underline{\underline{\kappa}}; \underline{\xi}) = m_p(\underline{\xi}) \, \|[J_2]\{\kappa\}\|
$$

where $[J_2] = \begin{bmatrix} 2/\sqrt{3} & 1/\sqrt{3} & 0 \\ 0 & 1 & 0 \\ 0 & 0 & 1/\sqrt{3} \end{bmatrix}$.

The contribution of the curvature term in the expression of the maximum resisting work (P_{rm}^{curv}) is then evaluated on the whole unit cell by a $n = 3$ points Gauss quadrature :

$$
P_{rm}^{curv} = \sum_{e=1}^{N_E} m_{p,e} \sum_{g=1}^{n} c_{e,g} \, \|[J_2]\{\chi\} + [J_2][B_{e,g}]\{V\}\|
$$

where $c_{e,g}$ are constant terms coming from the quadrature of the integral.

Since C^1-continuity is not assured, we have to take into account the contribution of rotation discontinuities across element edges to the maximum resisting work.

The support function associated to such discontinuities of normal rotation $\Delta\theta_n$ is :

$$
\pi(\Delta\theta_n; \underline{n}) = \pi(\underline{\underline{\kappa}} = \Delta\theta_n\underline{n} \otimes \underline{n}; \underline{\xi}) = \frac{2m_p(\underline{\xi})}{\sqrt{3}}|\Delta\theta_n|
$$

where the rotation discontinuity across edge j can be written :

$$
\Delta\theta_n = \langle \Delta\Theta_j \rangle \{V\}
$$

15

The contribution of rotation discontinuities in the expression of the maximum resisting work (P_{rm}^{disc}) is also evaluated over all N_D active[4] edges by a $m = n = 3$ points Gauss quadrature on the element edges :

$$P_{rm}^{disc} = \sum_{j=1}^{N_D} m_{p,j} \sum_{g'=1}^{m} c'_{j,g'} \, |\langle \Delta\Theta_j \rangle \{V\}|$$

where $c'_{j,g'}$ are constant terms coming from the quadrature of the integral and where $m_{p,j}$ is chosen as the minimum value of $m_p(\underline{\xi})$ over each side of edge j.

Finally, periodic boundary conditions (12) and (13) have to be satisfied. First, it is to be noticed that, since v admits a cubic interpolation over an element, it is not sufficient to impose that v is periodic at both end nodes of an edge for v to be periodic over the whole edge. Two supplementary conditions on the derivative of v along the edge have to be imposed. Hence, we must impose that $\partial_t v$ is periodic too. Therefore, since v and $\partial_t v$ must be periodic and $\partial_n v$ must be antiperiodic, it is equivalent to impose that v, $\partial_x v$ and $\partial_y v$ are periodic. For all pair (i, i') of opposite nodes, this can be written as :

$$\begin{Bmatrix} v_i \\ \partial_x v_i \\ \partial_y v_i \end{Bmatrix} - \begin{Bmatrix} v_{i'} \\ \partial_x v_{i'} \\ \partial_y v_{i'} \end{Bmatrix} = \{0\}$$

which leads to the condensed form $[P']\{V\} = \{0\}$.

5.2. Formulation as standard second-order cone programming

For a given value of $\underline{\underline{\chi}}$, the approximate macroscopic support function $\Pi_{hom}^{kin}(\underline{\underline{\chi}})$ is then obtained by solving the following optimization problem :

$$\Pi_{hom}^{kin}(\underline{\underline{\chi}}) = \quad \min \quad \sum_{e=1}^{N_E} m_{p,e} \sum_{g=1}^{n} c_{e,g} \, \|[J_2]\{\chi\} + [J_2][B_{e,g}]\{V\}\| + \sum_{j=1}^{N_D} m_{p,j} \sum_{g'=1}^{m} c'_{j,g'} \, |\langle \Delta\Theta_j \rangle \{V\}|$$
$$\text{s.t.} \quad [P']\{V\} = \{0\}$$

Introducing various auxiliary variables, the preceding problem can be reformulated as :

$$\begin{aligned} \Pi_{hom}^{kin}(\underline{\underline{\chi}}) = \quad &\min \quad \sum_{k=1}^{N_E \cdot n} m_{p,e} c_k t_k + \sum_{k'=1}^{N_D \cdot m} m_{p,j} c'_{k'} s_{k'} \\ &\text{s.t.} \quad [P']\{V\} = \{0\} \\ &\qquad [J_2]^{-1}\{r_k\} - [B_{e,g}]\{V\} = \{\chi\} \\ &\qquad t_k \geq \|\{r_k\}\| \\ &\qquad u_{k'} = \langle \Delta\Theta_j \rangle \{V\} \\ &\qquad s_{k'} \geq |u_{k'}| \end{aligned} \qquad (18)$$

---

[4]i.e. which actually contribute to P_{rm}^{disc}

which amounts to a standard SOCP problem involving linear equalities and inequalities, as well as $N_E \cdot n$ conic constraints.

Finally, since the curvature is exactly computed, and since conditions (10)-(13) are exactly satisfied over the whole unit cell, the following inclusion $KA_{0h} \subset KA_0$ holds true where KA_{0h} is the space of periodic fluctuations obtained with this discretization. Therefore, if numerical errors due to the quadrature of the integral can be neglected, it can be concluded that $\Pi_{hom}(\underline{\underline{\chi}}) \leq \Pi^{kin}_{hom}(\underline{\underline{\chi}})$ with Π^{kin}_{hom} being the support function of an upper bound approximation $G^{hom}_{kin} \supset G^{hom}$ of the macroscopic strength criterion.

6. Numerical examples

In the following, different examples of periodic plates will be treated such as reinforced or perforated plates. Lower and upper approximations will be computed by solving the static and kinematic approach on the unit cell using the methods presented in sections 4 and 5. Unit cells are meshed using GMSH, optimization problems (17) and (18) are formulated under the MATLAB environment and solved using the dedicated SOCP solver MOSEK [7]. For a given value of the macroscopic variables ($\underline{\underline{M}}$ or $\underline{\underline{\chi}}$), the resolution of the associated optimization problem derived from the static or the kinematic approach, took in general less than 1-2 seconds. Pre-processing including mesh generation and matrices assembling procedures took approximately 10-20 seconds.

6.1. Plate reinforced in one direction

The unit cell geometry represented in figure 6 corresponding to a plate made of a reference material of ultimate moment $m_{p1} = 1$ reinforced by a band of width $e = 0.05$ along the y direction made of a material of ultimate moment $m_{p2} = 40$ will first be considered.

A trivial static approach consisting of a homogeneous bending moment field $\underline{\underline{m}}(\underline{\xi}) = \underline{\underline{M}}$ shows that G^{hom} contains the domain defined by the von Mises criterion of the weakest material $m_{p1} = 1$, denoted by $G_{vM}(m_{p1})$. Similarly, a trivial kinematic approach with $v(\underline{\xi}) = 0$ (homogeneous curvature) shows that G^{hom} is contained in the domain defined by the von Mises criterion of average ultimate moment $\langle m_p \rangle = 0.95 \cdot 1 + 0.05 \cdot 40 = 2.95$, denoted by $G_{vM}(\langle m_p \rangle)$.

First, the intersection of G^{hom} with the plane $M_{xy} = 0$, noted $G^{hom}_{(xx,yy)}$ will be investigated. Due to the unit cell symmetry with respect to its center, it is easily shown that this intersection is also equal to the projection onto the plane $M_{xy} = 0$, which is also obtained by computing $\Pi_{hom}(\chi_{xx}, \chi_{yy}, \chi_{xy} = 0)$. Therefore, $G^{hom}_{(xx,yy)}$ is a convex domain of $\mathbb{R}^2$, the support function of which is given by $\Pi_{hom}(\chi_{xx}, \chi_{yy}, 0)$.

The results of both approaches are represented in figure 7. It can be observed that the points obtained from the static approach correspond exactly to the convex hull of the
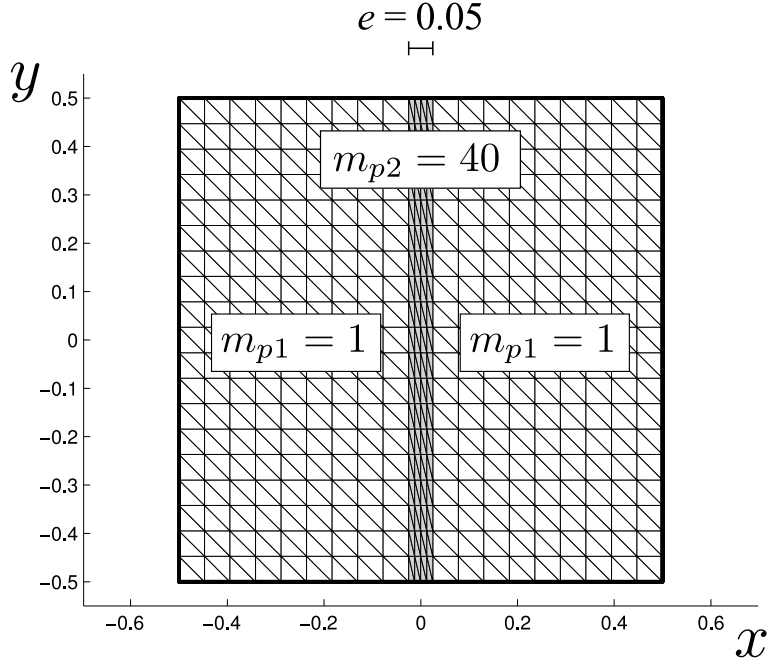
17

Figure 6: Geometry and mesh of the unit cell for the plate reinforced by periodic bands in the y-direction

tangent hyperplanes obtained from the kinematic approach, ensuring that $G^{hom}_{(xx,yy)}$ is exactly computed. As expected, the reinforcement is ineffective concerning bending moments along M_{xx}, only whereas for bending moments along M_{yy} only, the average strength $\langle m_p \rangle = 2.95$ is recovered.

Moreover, it is possible to show that $G^{hom}_{(xx,yy)}$ is actually given by the following analytical relations :

$$(M_{xx}, M_{yy}) \in G^{hom}_{(xx,yy)} \iff \exists(X, Y) \text{ such that } \begin{cases} (M_{xx}, X) \in G_{vM}(m_{p1}) \\ (M_{xx}, Y) \in G_{vM}(\langle m_p \rangle) \\ M_{yy} = (1 - \eta)X + \eta Y \end{cases}$$

where η is the fraction of the reinforcement, i.e. $\eta = e/a$. These relations mean that a point on $\partial G^{hom}_{(xx,yy)}$ is obtained as the barycenter of two points on $\partial G_{vM}(m_{p1})$ and $\partial G_{vM}(\langle m_p \rangle)$ which share the same abscissa M_{xx}, the weighting factor being given by $1 - \eta$ and η. This construction is very similar to the construction of the macroscopic strength criterion of a multilayer purely cohesive material under plane strain conditions [14].

In the limit of a small reinforcement fraction, $G^{hom}_{(xx,yy)}$ can be obtained by translating the von Mises ellipse with $m_p = 1$ (in red) by a vector ($M_{xx} = 0, M_{yy} = \pm 1.95$) which corresponds to the effect of the reinforcement along the direction y.

In figure 8, the whole domain G^{hom} has been represented in the (M_{xx}, M_{yy}, M_{xy}) space. Black dots correspond to points obtained from the static approach, whereas the gray domain
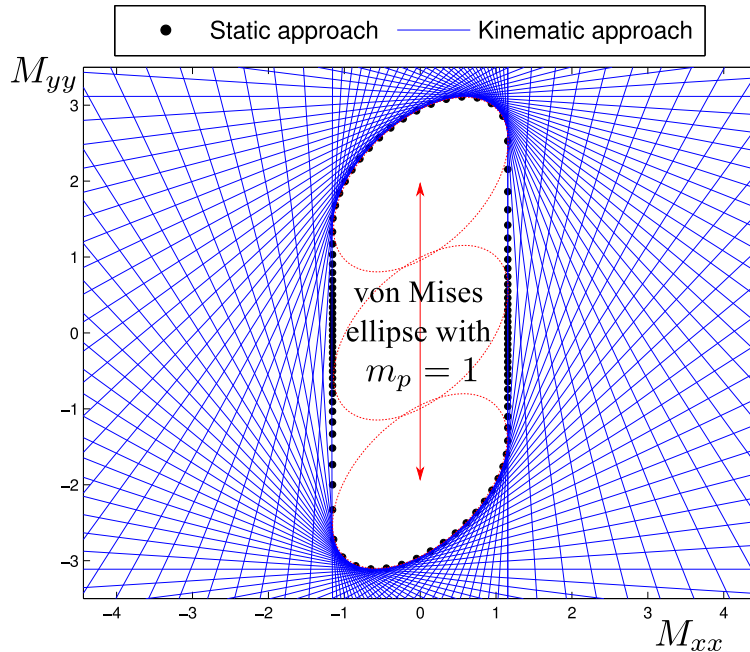
18

Figure 7: Domain $G^{hom}_{(xx,yy)}$ for the reinforced plate obtained by the static approach (black dots). Blue tangent planes are obtained with $\Pi_{hom}(\chi_{xx}, \chi_{yy}, 0)$ from the kinematic approach

correspond to the convex hull of the hyperplanes obtained from the kinematic approach. Clearly, both approaches lead to the same convex set with an excellent precision. It is also worth noting that G^{hom} has a relatively complex shape (which is not an ellipsoid) bounded by two planes of equation $M_{xx} = \pm \dfrac{2m_{p1}}{\sqrt{3}}$.

6.2. Plate perforated by a rectangular hole

The unit cell geometry represented in figure 9, corresponding to a plate made of a reference material of ultimate moment $m_{p1} = 1$ perforated by a rectangular hole of width $e = 0.1$ and length $l = 0.6$, will now be considered.

It is to be mentioned that this example involves a moment-free boundary (noted $\mathcal{B}$) inside the unit cell, which was not considered in the description of the auxiliary problem in section 3. The only modifications for the static approach are that the relations $m_{nn} = 0$ and $K = 0$ have to be imposed on $\mathcal{B}$. Concerning the kinematic approach, the only modification is that edges belonging to $\mathcal{B}$ remain inactive, i.e. they do not contribute to P^{disc}_{rm} via rotation discontinuities.

In figure 10, isovalues of the different components of the local bending moments $\underline{\underline{m}}(\underline{\xi})$ obtained by the static approach for a macroscopic bending moment of the form $\underline{\underline{M}} = \underline{e}_x \otimes \underline{e}_x$
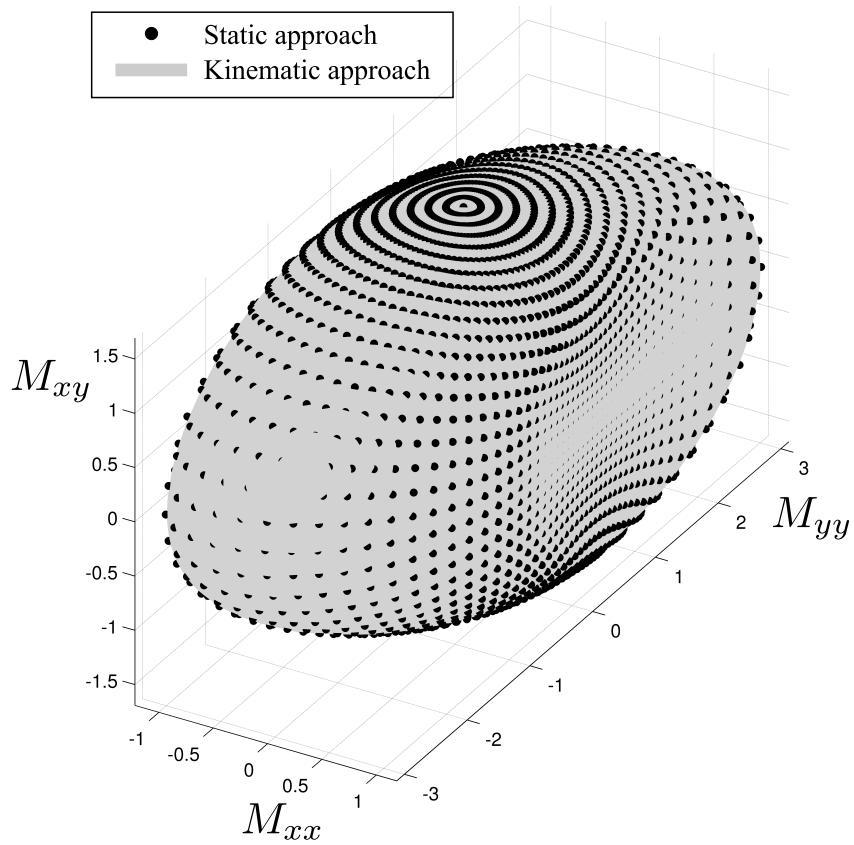
19

Figure 8: Domain G^{hom} for the reinforced plate obtained by the static approach (black dots). The grey domain is obtained as the convex hull of the hyperplanes obtained from the kinematic approach.
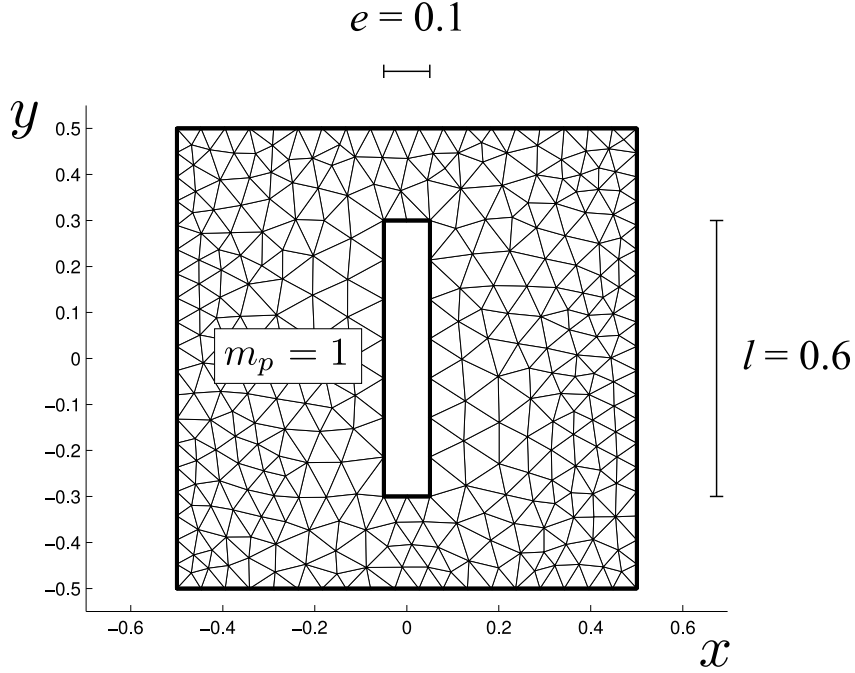
Figure 9: Geometry and mesh of the unit cell for the plate perforated by a rectangular hole

have been represented. It can be observed that the components satisfy all the conditions defining $SA(\underline{\underline{M}})$ (periodicity, boundary conditions on the free boundary, averaging relation,...). The complexity of the spatial variations of the local bending moment also underlines the need of numerical methods to solve the auxiliary problem, despite the simplicity of the macroscopic moment.

In figure 11, the failure mechanism (i.e. the field $u(\underline{\xi}) \in KA(\underline{\underline{\chi}})$) obtained by the kinematic approach has been represented for different values of the macroscopic curvature : pure curvature in the x-direction ($\chi_{xx} = 1, \chi_{yy} = \chi_{xy} = 0$), pure curvature in the y-direction ($\chi_{xx} = 0, \chi_{yy} = 1, \chi_{xy} = 0$) and pure $xy-$ torsion ($\chi_{xx} = \chi_{yy} = 0, \chi_{xy} = 1$). The mechanism obtained for $\chi_{xx} = 1$ in figure 10(a) corresponds to a yield line in the direction of the hole length. On the contrary for $\chi_{yy} = 1$ (figure 10(b)), a better mechanism than a simple yield line along the hole width is obtained via a complex local field with double curvature regions around the hole. Finally, for $\chi_{xy} = 1$ (figure 10(c)), the optimal mechanism seems to be a homogeneous torsion curvature field $u(\underline{\xi}) = \frac{1}{2}\underline{\xi} \cdot \underline{\underline{\chi}} \cdot \underline{\xi} = \xi_x \xi_y$ obtained with a zero periodic fluctuation $v(\underline{\xi}) = 0$. Those results also illustrate the complexity of the auxiliary problem, justifying the use of numerical methods to solve the static as well as the kinematic approach.

Finally, in figure 12 the intersection of G^{hom} with the plane $M_{xy} = 0$ has been represented for various values of the hole length l while keeping the hole width equal to $e = 0.1$.
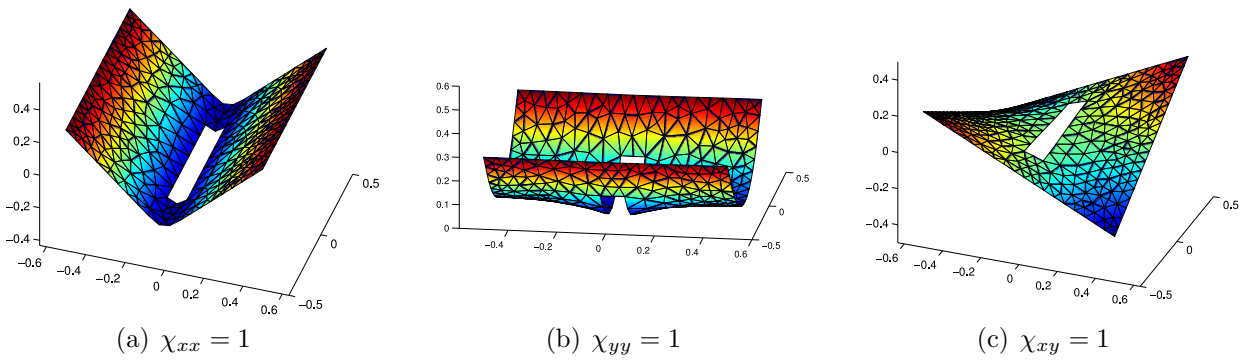
21
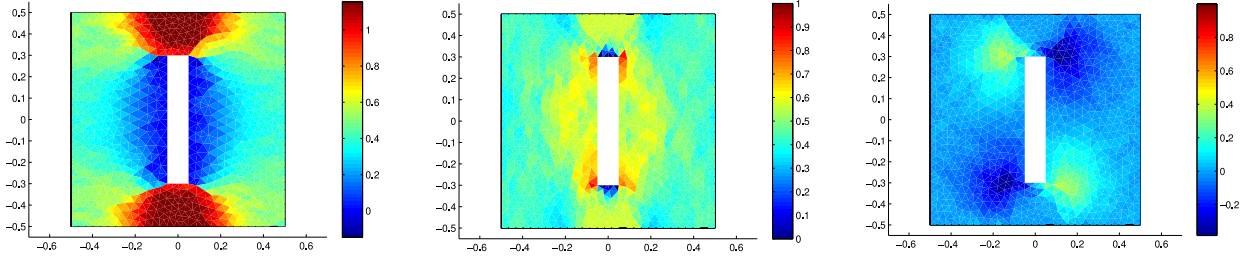
(a) m_{xx} component   (b) m_{yy} component   (c) m_{xy} component

Figure 10: Mapping of the local bending moment $\underline{\underline{m}}(\underline{\xi})$ for a macroscopic bending moment of the form $\underline{\underline{M}} = \underline{e}_x \otimes \underline{e}_x$

(a) $\chi_{xx} = 1$ (b) $\chi_{yy} = 1$ (c) $\chi_{xy} = 1$

Figure 11: Failure mechanism of the unit cell for different values of the macroscopic curvature
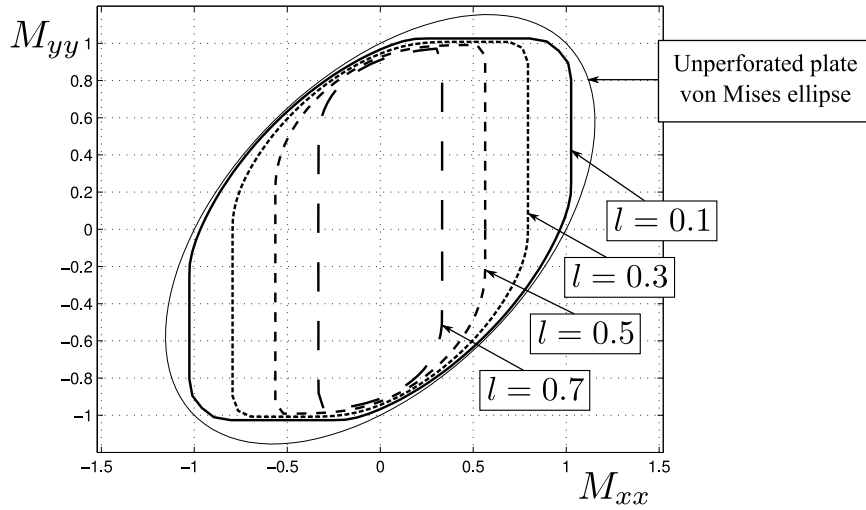
Figure 12: Domain $G^{hom}_{(xx,yy)}$ for different values of the hole length l

6.3. Influence of the arrangement pattern of circular holes in a perforated sheet

Perforated metal sheets are frequently used in the steel industry, offering a large variety of hole shapes (round, square, slotted,...), opening area percentage and pattern arrangement. In this example, it seemed interesting to study the influence of pattern arrangement in the case of circular holes. Holes can, for example, be disposed in staggered rows or in straight rows. The ultimate bending strength can be estimated by solving the problem of an infinite plate solicited by a bending moment at infinity, or equivalently, by solving the auxiliary yield design problem on the unit cell with this bending moment as the macroscopic loading. Hence, in the following, the auxiliary problem will be solved to assess the ultimate strength in bending of those plates for different hole patterns.

Different unit cell geometries are considered in function of the pattern angle θ. The pattern geometries are obtained by translating circular holes of radii R along vectors $\underline{a}_1 = a\underline{e}_x$ and $\underline{a}_2 = a\sin\theta\underline{e}_x + a\cos\theta\underline{e}_y$ (see figure 13). The unit cell area is then $|\mathcal{A}| = a^2\cos\theta$. The opening area ratio (or porosity) is defined as $\eta = \pi R^2/|\mathcal{A}|$. Since we want to investigate the influence of the pattern angle on the macroscopic strength properties, a constant opening area ratio will be assumed for different values of θ. Hence, the radius R is set to $R = R_0\sqrt{\cos\theta}$ where R_0 is the hole radius for $\theta = 0$ such that $\eta = \pi R_0^2/a^2$ is now independent of θ.

Due to the chosen geometry, the strength capacity which will be most influenced by the pattern angle is the maximum bending moment in the $x-$direction, denoted by $M_{xx,0}$ and defined as :

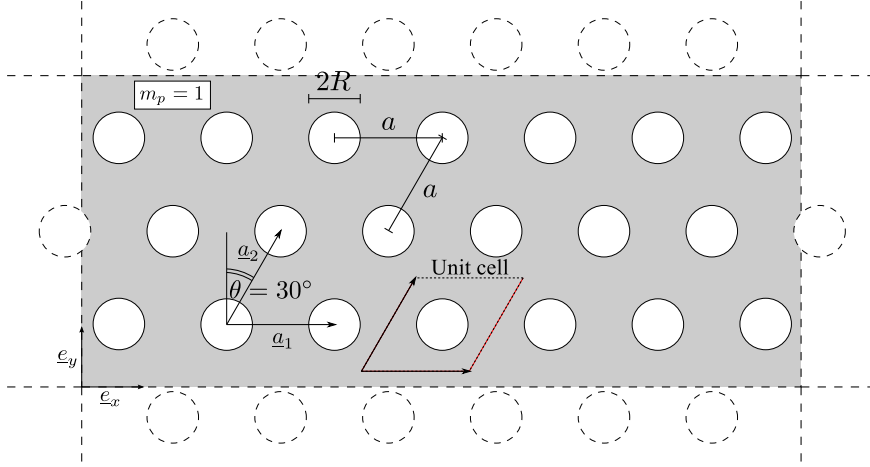$$M_{xx,0} = \max_{\underline{\underline{M}} = M\underline{e}_x \otimes \underline{e}_x \in G^{hom}} M$$

23

Figure 13: Perforated plate geometry for a $\theta = 30°$ pattern angle

This quantity has been computed using the static approach for varying values of θ. In figure 14, the variation of $M_{xx,0}$ as a function of pattern angle θ is represented. Three different values of the opening area ratio have been considered : $\eta = 0.03$, $\eta = 0.13$ and $\eta = 0.28$. Obviously, for a non-perforated plate ($\eta = 0$), we have $M_{xx,0} = m_p = 1$. Results indicate that $M_{xx,0}$ is decreasing with increasing values of η but the evolution of $M_{xx,0}$ with respect to θ is non-monotonous. Besides, the influence of the pattern angle is increasing with η. In particular, for $\eta = 0.28$, the staggered 30° pattern has a reinforcing effect of approximately 30% compared to the straight pattern ($\theta = 0°$). This reinforcement effect is around 15% for $\eta = 0.13$ but only 2% for $\eta = 0.03$. Therefore, the pattern arrangement may have a non-negligible reinforcing effect on the homogenized strength capacities of the plate for high opening area ratios.

Now, defining $\underline{e}_\alpha = \cos\alpha \underline{e}_x + \sin\alpha \underline{e}_y$, the ultimate bending moment in the α-direction $M_{\alpha\alpha,0}$ is defined as :

$$M_{\alpha\alpha,0} = \max_{\underline{\underline{M}} = M\underline{e}_\alpha \otimes \underline{e}_\alpha \in G^{hom}} M$$

It is interesting to note that in the case of a straight pattern ($\theta = 0°$), $M_{\alpha\alpha,0}$ tends to increase with α from $0°$ to $45°$ and to decrease symmetrically (due to the orthogonal symmetry of the problem) from $45°$ to $90°$ (figure 15(a)). This effect can be explained because the smallest path between two holes in the orthogonal direction of the loading is equal to a for $\alpha = 0°$ or $90°$ and equal to $\sqrt{2}a$ for $\alpha = 45°$. On the contrary, in the case of staggered pattern ($\theta = 30°$), $M_{\alpha\alpha,0}$ decreases with α from $0°$ to $30°$ and then decreases symmetrically (due to the hexagonal symmetry of the problem) from $30°$ to $60°$ (figure 15(b)). In this case, the smallest path is larger than a for $\alpha = 0°$ or $60°$, whereas it is equal to a for $\alpha = 30°$. Hence, for the straight pattern the optimal loading direction seems to be around $45°$ whereas for the staggered pattern the optimal loading direction is aligned with the holes.

Finally, the intersection of G^{hom} with the plane $M_{xy} = 0$ has been represented in figure 16 for $\eta = 0.13$ and two values of the pattern angle : $\theta = 0°$ and $\theta = 30°$. The reinforcing

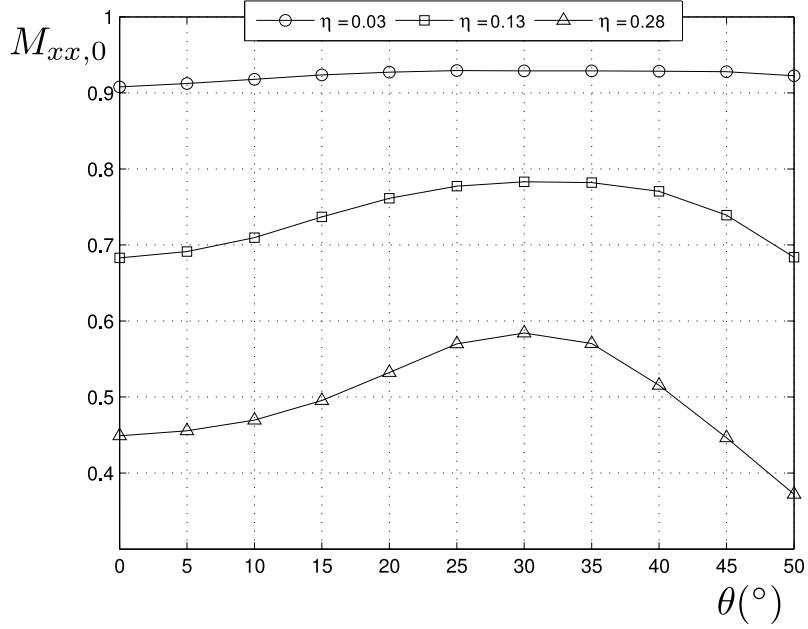Figure 14: Variation of $M_{xx,0}$ as a function of pattern angle θ for different values of the opening area ratio
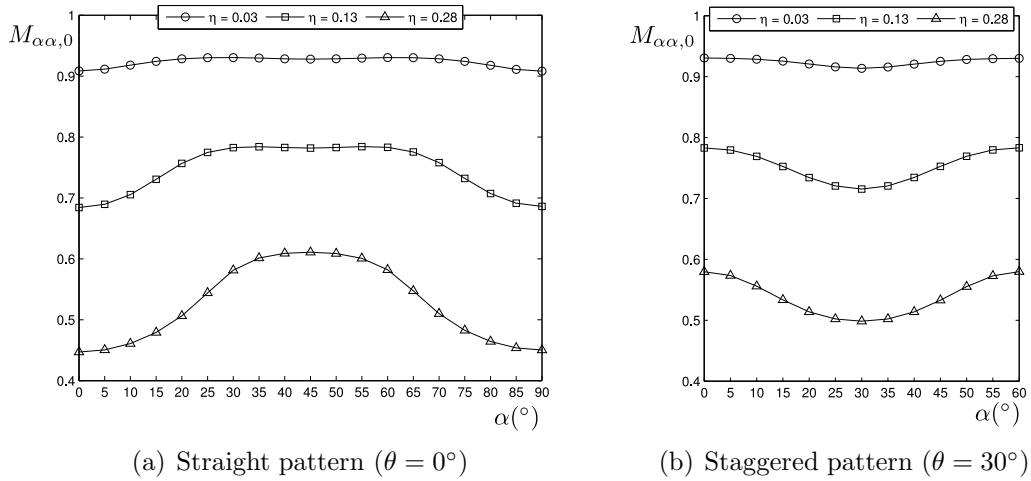

(a) Straight pattern ($\theta = 0°$)

(b) Staggered pattern ($\theta = 30°$)

Figure 15: Variation of $M_{\alpha\alpha,0}$ as a function of loading direction α for the straight and staggered pattern
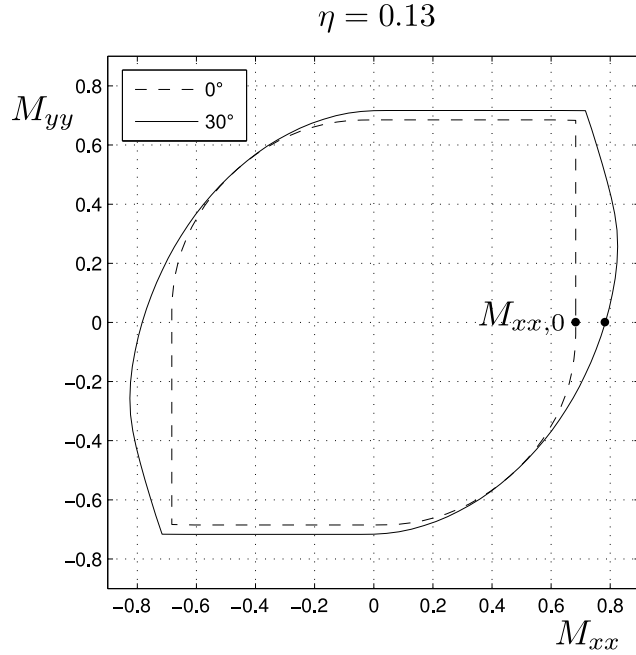
25

Figure 16: Domain $G^{hom}_{(xx,yy)}$ for $\theta = 0°$ and $\theta = 30°$ (with $\eta = 0.13$)

effect of the 30° pattern, compared to the straight pattern, can clearly be observed, not only for the particular value of $M_{xx,0}$, but also for the whole strength domain.

7. Conclusion

Yield design of thin periodic plates in bending has been addressed using a homogenization procedure to derive the macroscopic strength criterion of an equivalent homogeneous plate. The macroscopic strength criterion is obtained by solving an auxiliary yield design problem formulated on the unit cell characterizing the periodic microstructure. Static and kinematic approaches are formulated using a thin plate model, which is valid in the limit $h \ll a$ of a small plate thickness h compared to the unit cell characteristic length a. Numerical tools are introduced to solve both approaches efficiently in terms of computational time and accuracy. Indeed, the discrepancy between the evaluation of the macroscopic domain obtained from the two different approaches was negligible for all examples. The global efficiency and performance of the proposed method is based upon the following decisive ingredients :

- The discretization of the static approach is performed with finite elements satisfying exactly all equilibrium equations, periodic boundary conditions and local yield criterion.

- The discretization of the kinematic approach is performed with non-conforming finite elements, whose performance regarding upper bound limit analysis of thin plates had previously been demonstrated in [12].

26

- The related optimization problems are formulated as standard SOCP problems for which a dedicated software package has already been successfully employed for solving yield design problems.

It has been shown on various examples that the macroscopic strength criteria are usually complicated anisotropic three-dimensional surfaces in the space of bending moments. Therefore, even if such criteria can be obtained by efficient numerical procedures as those presented in this paper, the main difficulty of homogenization theory in yield design relies on the implementation of such complex criteria in a yield design problem formulated on the global structure. Approximate representations of those yield criteria are, therefore, required to perform such computations. This specific aspect will be the purpose of the second part of this work.

References

[1] J. Salençon, Yield Design, Wiley. com, 2013.

[2] E. Faccioli, E. Vitiello, A finite element, linear programming methods for the limit analysis of thin plates, International Journal for Numerical Methods in Engineering 5 (1973) 311–325.

[3] J. Munro, A. Da Fonseca, Yield line method by finite elements and linear programming, Structural Engineer 56 (1978) 37–44.

[4] S. Sloan, Lower bound limit analysis using finite elements and linear programming, International Journal for Numerical and Analytical Methods in Geomechanics 12 (1988) 61–77.

[5] S. Sloan, Upper bound limit analysis using finite elements and linear programming, International Journal for Numerical and Analytical Methods in Geomechanics 13 (1989) 263–282.

[6] K. D. Andersen, E. Christiansen, M. L. Overton, Computing limit loads by minimizing a sum of norms, SIAM Journal on Scientific Computing 19 (1998) 1046–1062.

[7] Mosek, The Mosek optimization toolbox for MATLAB manual, 2008.

[8] A. Makrodimopoulos, Remarks on some properties of conic yield restrictions in limit analysis, International Journal for Numerical Methods in Biomedical Engineering 26 (2010) 1449–1461.

[9] A. Makrodimopoulos, C. Martin, Upper bound limit analysis using simplex strain elements and second-order cone programming, International Journal for Numerical and Analytical Methods in Geomechanics 31 (2007) 835–865.

[10] H. Ciria, J. Peraire, J. Bonet, Mesh adaptive computation of upper and lower bounds in limit analysis, International Journal for Numerical Methods in Engineering 75 (2008) 899–944.

[11] C. Le, H. Nguyen-Xuan, H. Nguyen-Dang, Upper and lower bound limit analysis of plates using FEM and second-order cone programming, Computers & Structures 88 (2010) 65–73.

[12] J. Bleyer, P. de Buhan, On the performance of non-conforming finite elements for the upper bound limit analysis of plates, International Journal for Numerical Methods in Engineering 94 (2013) 308–330.

[13] P. Suquet, Elements of homogenization for inelastic solid mechanics, Homogenization techniques for composite media 272 (1985) 193–278.

[14] P. de Buhan, A fundamental approach to the yield design of reinforced soil structures, Ph.D. thesis, Thèse d'Etat, Paris VI, 1986.

[15] S. Bourgeois, Modélisation numérique des panneaux structuraux légers, Ph.D. thesis, Université d'Aix-Marseille 2, FRANCE, 1997.

[16] K. Sab, Yield design of thin periodic plates by a homogenization technique and an application to masonry walls, Comptes Rendus Mecanique 331 (2003) 641–646.

[17] J. Dallot, K. Sab, Limit analysis of multi-layered plates. Part I: the homogenized Love–Kirchhoff model, Journal of the Mechanics and Physics of Solids 56 (2008) 561–580.

[18] G. Duvaut, A. Metellus, Homogénéisation d'une plaque mince en flexion de structure périodique et symétrique, Comptes Rendus de l'Académie des Sciences, Paris 283 (1976) 947–950.

[19] T. Lewiński, J. J. Telega, Plates, laminates, and shells: asymptotic analysis and homogenization, volume 52, World Scientific, 2000.

[20] J. Salençon, Handbook of Continuum Mechanics: General Concepts, Thermoelasticity, Physics and Astronomy Online Library, Springer, 2001.

[21] P. Olsen, The influence of the linearisation of the yield surface on the load-bearing capacity of reinforced concrete slabs, Computer Methods in Applied Mechanics and Engineering 162 (1998) 351–358.